JWST-STScI-005934
SM-12

STScI | SPACE TELESCOPE SCIENCE INSTITUTE

JWST TECHNICAL REPORT

Title: Title: NIRISS Target Acquisition: the sensitivity of centroid accuracy to the presence of saturated pixels	Doc #: JWST-STScI-005934, SM-12 Date: 31 August 2017 Rev: -
Authors: Paul Goudfrooij Phone: 410 338-4981	Release Date: 14 September 2017

1. Abstract

We describe the sensitivity of the centroiding algorithm within the `GENTALOCATE` script used for on-board target acquisition (TA) to saturated pixels within the point spread function (PSF) of bright stars. The simulations use NIRISS PSFs that are centered on various locations within a detector pixel, and saturation is introduced at various stages during an integration. For TAs that use direct imaging with the F480M filter, we find the centroiding to be relatively insensitive to saturation unless it occurs before a fraction (N+1)/2N of the integration's duration (defined here as 'hard' saturation). Conversely, TAs that use the NRM element in the pupil wheel can incur centroid errors of 1.0 pixels or more when 4 or more pixels in the PSF are saturated. We recommend that TAs with NIRISS are executed with maximum numbers of 'partially' saturated pixels of 5 and 3 for CLEARP and NRM PSFs, respectively. We also make specific recommendations on which NIRISS TA mode to use for observations in the SOSS and AMI modes for a given target brightness.

2. Introduction: NIRISS Target Acquisitions

Target acquisitions (hereafter TAs) are supported for two NIRISS observing modes: Single-Object Slitless Spectroscopy (SOSS: Goudfrooij et al. 2014a) and Aperture Masking Interferometry (AMI: Goudfrooij et al. 2014b; Sivaramakrishnan & Artigau 2014). In both modes, TAs are required when a subarray is used for the science observations[1]. The reason for using TAs in these modes is the need to position the source at the best possible accuracy within a specific pixel of the detector. The main underlying reason is that many science projects using SOSS and AMI, such as observations of (transiting) exoplanets around nearby stars, will require noise levels of order only tens of parts per million, which is infeasible using pixel-by-pixel flatfielding (Goudfrooij, Albert & Doyon 2015a). The goal is therefore to position the target always on the same detector pixel, hence the need for accurate TAs.

Typical targets for SOSS and AMI observations are expected to be nearby stars, which can be

[1] SOSS and AMI modes also allow full-frame observations which do not require TAs.

very bright. As such, it is important to study the impact saturation can have on the centroiding accuracy of NIRISS TAs. This is the subject of this report. After a brief description of the TA algorithm in Section 3, our tests of the sensitivity of the centroiding algorithm to various levels of saturation are described and illustrated in Section 4. Section 5 contains our recommendations for SOSS and AMI TAs, and our findings are summarized in Section 6.

3. The JWST Target Acquisition Algorithm `GENTALOCATE`

JWST TAs will be performed on-board using a stored commanding script called `GENTALOCATE`. The latter is based on the "centered window first moment" algorithm written by Mike Regan and described in detail in Valenti et al. (2013). Here we just include a brief summary of the main steps of this algorithm. The procedure starts by finding the brightest "central pixel" in the TA subarray using a checkbox of N × N pixels (3 × 3 in case of NIRISS TAs) that is moved across the full subarray while recording the total intensities within each checkbox. This process is followed by creating a "raster window" of M × M pixels (5 × 5 in case of NIRISS TAs) which is centered on the central pixel of the brightest checkbox found in the previous step. The centroid of the object in the raster window is then computed by calculating the first moment of the intensity distribution. The raster window is then centered on the newly found center, and the center is re-computed. This iterative process is continued until either a convergence threshold is achieved, or until a given maximum number of iterations has been performed.

It was recently realized that the centering accuracy of the original `GENTALOCATE` algorithm was susceptible to effects of bad pixels (either dead pixels or hot pixels) if the latter are located in particular regions around the center of the point spread function (PSF). Details on this are described in reports by Goudfrooij et al. (2015b) and Holfeltz, Goudfrooij, & Sivaramakrishnan (2015). In response to their findings, the `GENTALOCATE` script was expanded, adding new input parameters to allow three bad pixel mitigation strategies (see Goudfrooij et al. 2015b for details). The selection of the `GENTALOCATE` parameter values used in NIRISS TA modes is described in Goudfrooij et al. (2016).

4. The Effects of Saturated Images in `GENTALOCATE` Processing

To enable cosmic ray rejection in TA exposures, `GENTALOCATE` selects 2, 3, or 8 "images" (corresponding to groups) read out during an integration ramp for further processing (see Valenti et al. 2013). In this report, we only address the (most common) case when 3 such images are selected by `GENTALOCATE`, and that the number of groups in an integration is odd. For that case, `GENTALOCATE` selects the following groups as "images": 1, (N+1)/2, and N, where N is the value of NGROUPS, i.e., the number of groups read out during an integration ramp. We designate those respective "images" as `im1`, `im2`, and `im3` in the following. For the execution of the centroiding procedure, `GENTALOCATE` creates an image "`ta_image`":

```
ta_image = min((im3−im2), (im2−im1)).
```

The implication of this procedure is that saturation occurring during a TA exposure can have two (significantly different!) effects on this image `ta_image`:

a) If saturation occurs in the period *after* group `im2` is read out, then the central pixel(s) of the PSF will be depressed in the difference image `(im3−im2)` relative to the image `(im2−im1)`. Consequently, the central pixels of the PSF in image

`ta_image` will be taken from `(im3-im2)` and hence have somewhat lower values than they would have in case of no saturation, thus causing a "flat-topped" light distribution. We refer to this type of saturation as "partial" saturation.

b) On the other hand, if saturation occurs at a time *before* group `im2` is read out, then the central region of the PSF will have image values close to zero in the difference image `(im3-im2)`, since no electrons could further accumulate in the saturated pixel(s) after group `im2` was read out. Consequently, the central pixels of the PSF in image `ta_image` will be taken from image `(im3-im2)` and hence be rendered with values close to zero. ***This effect can cause very significant centroid errors***, especially in case of PSFs that are not well centered on a pixel. We call this "hard" saturation. An example of this is shown in the left panel of Figure 1 below, which shows the image `ta_image` in a simulated case where the PSF is centered near the corner of a pixel and saturation occurred just less than halfway between the times when groups `im1` and `im2` were read out.

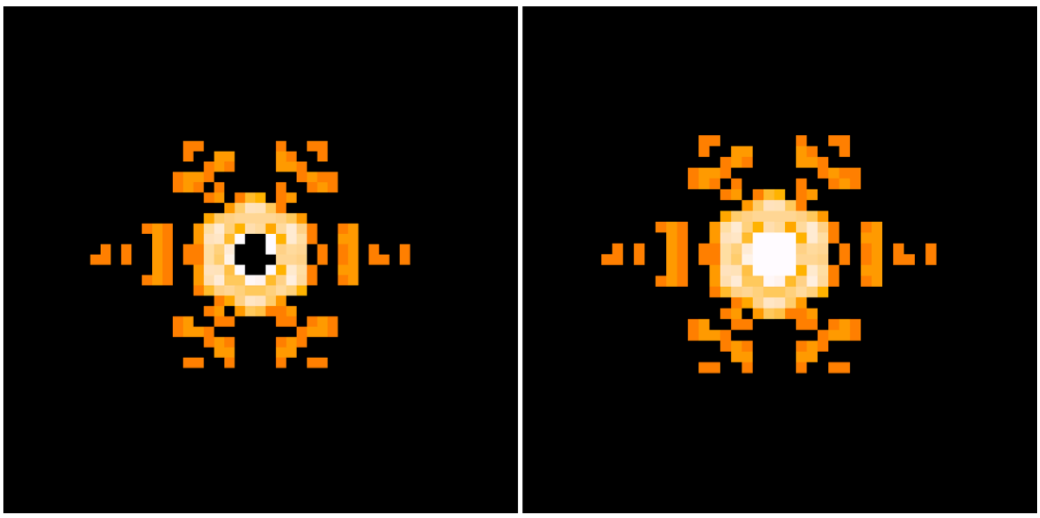

Figure 1. Left panel: simulated 3.1 × 3.1 arcsec^2 image resulting from GENTALOCATE processing of a TA exposure during which the peak pixel of a NIRISS CLEARP/F480M PSF saturated the detector during the first half of an integration (so-called "hard" saturation). Right panel: Same PSF as in left panel, but now for an exposure *without* saturated pixels (shown for comparison purposes). Both panels use the same logarithmic intensity scale to highlight the full extent of the PSF.

Quantifying the effects of saturation in terms of centroid errors

To quantify the range of centroid errors that can result from the effects of saturation mentioned above, we conduct a suite of simulations that utilize PSFs created by means of the WebbPSF Python package (Perrin et al. 2014), using an assumed optical path difference between the telescope mirror segments of 162 nm rms. The different PSFs were centered on a wide variety of pixel phases (or locations within a pixel) to simulate the randomness of the actual in-flight situation. As such, a grid of 19×19 PSFs were created for pupil/filter wheel combinations CLEARP/F480M and NRM/F480M, corresponding to the "FAINT" and "BRIGHT" TA modes of NIRISS available in the Astronomers Proposal Tool (APT),

respectively. The NRM element in the pupil wheel is an aperture mask with 7 "holes" that produce an interferogram in the image plane, sampling 21 unique ("non-redundant") baselines and resulting in 6 distinct interferometric fringes in the outskirts of the PSF (see Goudfrooij et al. 2014b). Its advantage in the context of TAs of bright targets is that its throughput is only ~15% of that of the CLEARP element in the pupil wheel, while providing a PSF that is actually more strongly peaked in its center (Goudfrooij et al. 2016). Different levels of saturation were simulated by letting the peak pixel of the PSF saturate at 6 different times during the integration on a "saturation time" scale from 1.0 to 3.0, corresponding to the times when groups `im1` and `im3` (as defined above) are read out. (Figure 2 illustrates how groups read out during an integration correspond to this "saturation time" scale.) Pixels surrounding the peak pixel of the PSF continue to accumulate charge (or intensity) until they reach the level of the peak pixel (if ever). The number of pixels that saturate during the exposure and the input central (X, Y) coordinates of the PSF are tracked in FITS header keywords of the output image, which corresponds to the image `ta_image` as defined above. Finally, we run an implementation of the `GENTALOCATE` centroid algorithm rendered in IDL[2] on each such simulated image, using `GENTALOCATE` parameter values appropriate for NIRISS TAs.

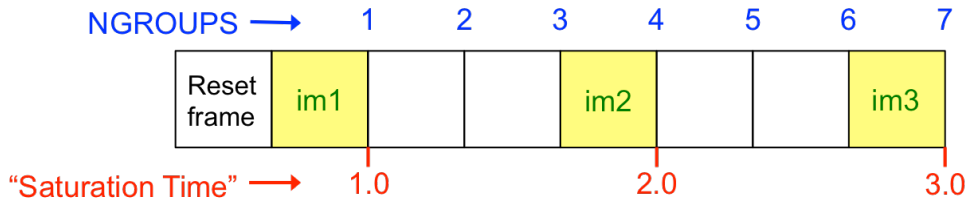

Figure 2. Schematic illustration of a TA integration of 7 groups. The relations between NGROUPS, groups 'im1', 'im2', and 'im3', and the "Saturation Time" as mentioned in the text are indicated.

Figure 3 below shows the results of the simulations expressed as centroid error as a function of the number of pixels that saturated during the exposure. The top and bottom panels of Figure 3 refer to the cases when the saturation during the exposure in question was "partial" and "hard" (i.e., saturation cases (a) and (b) mentioned above), respectively. The left-hand and right-hand panels show the results for two different ranges of the abscissa and ordinate.

Among the simulations of "partially" saturated CLEARP/F480M PSFs, Figure 3 shows that the centroid error stays well within 0.1 pixel for cases of up to 6 saturated pixels. This corresponds to the case where saturation occurs exactly at the time when group `im2` is being read out (i.e., "saturation time" = 2.0, the "middle" group up the integration ramp of the TA exposure, cf. above). Conversely, when saturation becomes "hard" for CLEARP/F480M PSFs, centroid errors quickly rise above a level of 0.1 pixel. As such, one can expect high-S/N CLEARP/F480M centroids to be accurate to within ~0.05 pixel if saturation occurs at or after a fraction (N+1)/2N of the integration time, where N is the value of NGROUPS.

For NRM PSFs, the effects of saturation are found to be more severe than for CLEARP PSFs. This is especially the case for "hard" saturation. This difference is due in part to the moderate asymmetry of the NRM PSF around its center, and in part to its relatively narrow central peak (see, e.g., Goudfrooij et al. 2014b). However, the centroid errors for saturated

[2]This script is based on the FORTRAN code by Anderson (2008).

NRM PSFs stay within ~0.1 pixel as long as the number of partially saturated pixels stays below or equal to 3. This corresponds to the case where saturation occurs at a time approximately halfway between the times when groups `im2` and `im3` are read out, depending on where the PSF is centered within a pixel (specifically, we find a range of "saturation times" of 2.3 − 2.6). In terms of AMI-mode science observations which use the SUB80 subarray of 80×80 pixels, this corresponds to a range of 1.4 – 1.6 SUB80 groups. Thus, saturation-related problems with AMI/NRM TAs are only expected for sources that saturate in two SUB80 frames, corresponding to sources with 4.8 μm magnitudes ≤ 2.9 in the Vegamag system[3] (Goudfrooij et al. 2016).

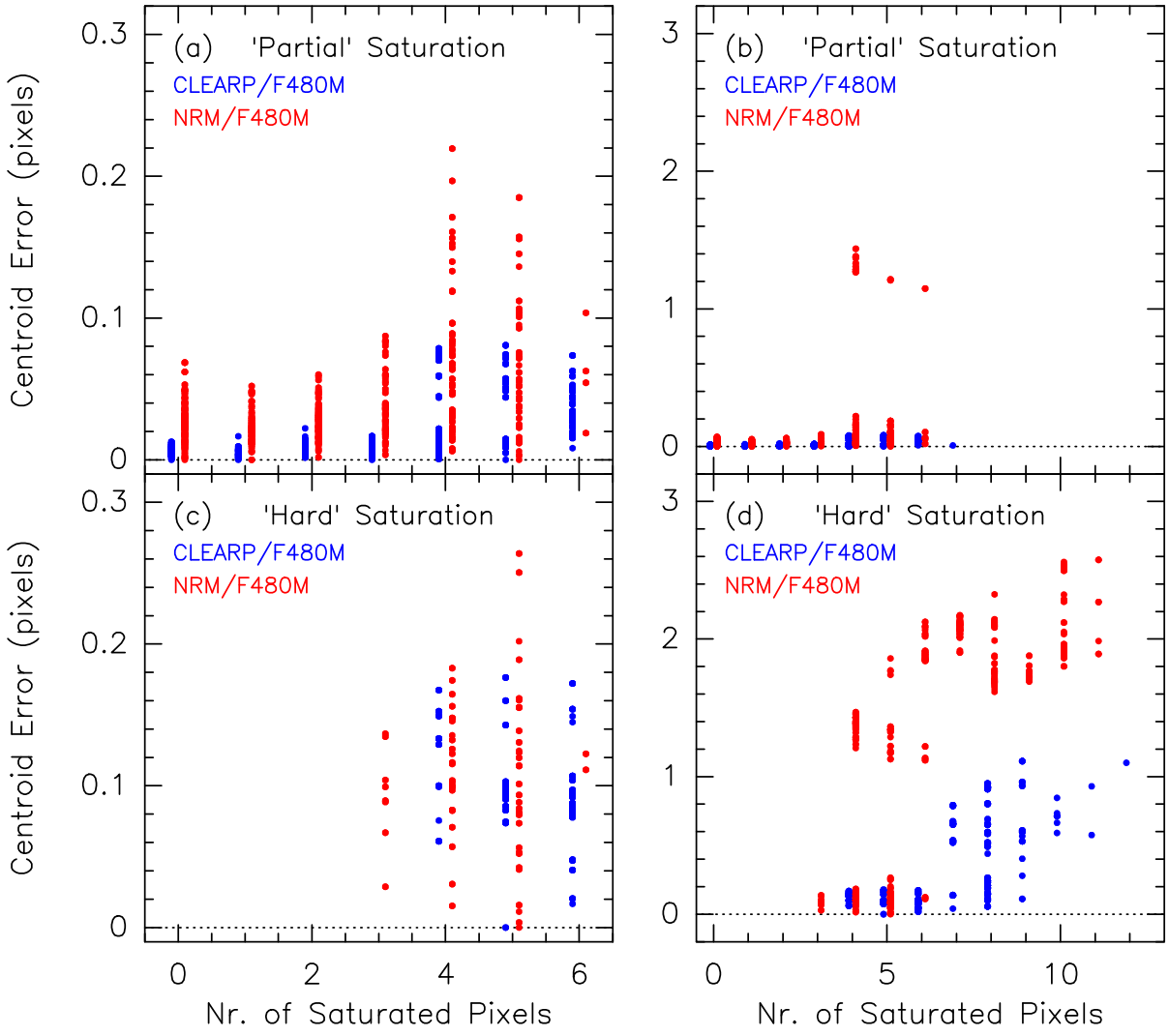

Figure 3. Centroid error versus the number of saturated pixels incurred during the various simulated exposures described in §4. Results for CLEARP/F480M and NRM/F480M PSFs are shown in blue and red, respectively. The top panels [(a) and (b)] represent cases where the saturation was "partial"

[3] One should consider using "offset targets" for AMI TAs of such bright stars.

whereas the bottom panels [(c) and (d)] represent cases of "hard" saturation. The left-hand and right-hand panels show the results for two different ranges along the abscissa and ordinate. In the left-hand panels, the symbols associated with the two types of PSFs (blue vs. red symbols) are plotted with a small relative offset along the abscissa for clarity purposes.

5. Recommendations for SOSS and AMI Target Acquisitions

As already mentioned above, NIRISS allows two modes of TA, designated as the "FAINT" and "BRIGHT" TA modes in APT. These correspond to the pupil/filter wheel combinations CLEARP / F480M and NRM / F480M, respectively. While the "FAINT" vs. "BRIGHT" classification refers to the fact that the light throughput of the NRM pupil wheel element is only ~15% of that of the CLEARP element, there is also another consideration to be made in the choice between the two TA modes, namely the fact that the NRM element exposes only (part of) 7 of the 18 segments of JWST's primary mirror (PM), whereas the CLEARP element exposes almost the full PM. As shown by Holfeltz, Sivaramakrishnan, & Goudfrooij (2015), this causes a difference between the centroid locations of CLEARP and NRM PSFs of up to a few tenths of a pixel, depending on the specifics of the optical path differences between the various PM segments in flight. The (potential) impact of this difference is described below in the context of the SOSS and AMI observing modes.

5.1. SOSS Target Acquisitions

The pupil wheel element used for SOSS science spectra is the GR700XD grism, which is mounted in a square aperture mask that blocks the outer segments of the JWST PM. As such, its field of regard is much more akin to that of the CLEARP element than to that of the NRM (since the latter exposes only outer PM segments). Furthermore, the NIRISS Commissioning of the SOSS mode will be done with targets that will be in the brightness range appropriate for CLEARP TAs. These observations will define the default location of the spectral trace for the SOSS mode and the associated reference files for the JWST calibration pipeline. As such, we generally recommend to use CLEARP (rather than NRM) TAs for SOSS observations if at all possible given the brightness of the science target. As mentioned in §4 above, CLEARP TAs are safe up to the source brightness for which saturation occurs at "saturation time" = 2.0, which corresponds to 2 groups for a 64×64 (TA) subarray exposure with NGROUPS = 3 (which is the smallest supported value of NGROUPS for NIRISS TAs). According to the NIRISS Exposure Time Calculator (ETC), this limit is reached for a point source with a F480M magnitude of 6.1 in the Vega-based system, corresponding to an AB magnitude of 9.6 or a flux density of 0.54 Jy at 4.8 μm. Consequently, we only recommend using the NRM ("BRIGHT") TA mode for SOSS observations for sources brighter than that limit.

5.2. AMI Target Acquisitions

Since AMI science exposures are taken with the NRM in place, we recommend using the NRM ("BRIGHT" in APT) TA mode for AMI observations unless the source is too faint to reach a S/N of 30 in NGROUPS = 19. According to the NIRISS ETC, S/N = 30 is reached for a point source with F480M = 9.3 Vegamag, corresponding to AB = 12.8 mag and a flux density of 28.6 mJy at 4.8 μm. For sources fainter than that limit, we recommend switching to the "FAINT" TA mode that uses the CLEARP pupil wheel element.

6. Summary and Conclusions

We describe the sensitivity of the centroiding algorithm within the GENTALOCATE script

used for on-board TAs to saturated pixels within the PSF of bright stars. The simulations use NIRISS PSFs that are centered on various locations within a detector pixel, and saturation is introduced at various stages during an integration. For TAs that use direct imaging (i.e., the CLEARP pupil wheel element, corresponding to the "FAINT" TA mode in APT) with the F480M filter, we find the centroiding to be relatively insensitive to saturation unless it occurs before a fraction (N+1)/2N of the integration's duration (where N is the value of NGROUPS). Conversely, TAs that use the NRM element in the pupil wheel (the "BRIGHT" TA mode in APT) can incur large centroid errors of 1.0 pixels or more if 4 or more pixels in the PSF are saturated. The latter occurs when saturation sets in approximately halfway through the last group in the integration. We recommend that TAs with NIRISS be executed with maximum numbers of saturated pixels of 5 and 3 for CLEARP and NRM PSFs, respectively.

We clarify that centroid locations of NRM PSFs can differ from those of CLEARP PSFs (for a given telescope pointing) by up to a few tenths of a pixel, depending on the specifics of the optical path differences between the various PM segments in flight. We discuss the impact of this effect and come up with recommendations for when to use the "BRIGHT" vs. the "FAINT" TA modes for observations in the SOSS and AMI mode. For SOSS observations, we recommend use of the "FAINT" TA mode unless the target is brighter than 0.54 Jy at 4.8 μm. For AMI observations, we recommend use of the "BRIGHT" TA mode unless the target is fainter than 28.6 mJy at 4.8 μm.

7. References

Anderson, J., 2008, "How the Color of a Star May Affect Guide Star Centering", JWST Technical Report JWST-STScI-001499

Goudfrooij, P., Albert, L., et al. 2014a, "NIRISS Operations Concepts: The Single-Object Slitless Spectroscopy mode", JWST Technical Report JWST-STScI-003577

Goudfrooij, P., Artigau, E., Sivaramakrishnan, A., et al. 2014b, "NIRISS Operations Concepts: The Aperture Masking Interferometry mode", JWST Technical Report JWST-STScI-003576

Goudfrooij, P., Albert, L., & Doyon, R., 2015a, "The Single-Object Spectroscopy Mode of *Webb*'s NIRISS Instrument", STScI Newsletter, Vol. 32, Issue 01, pp. 37-39

Goudfrooij, P., Holfeltz, S., Hilbert, B., Stansberry, J., Keyes, T., & Hines, D., 2015b, "The GENTALOCATE Algorithm for JWST Target Acquisitions: Its Sensitivity to the Presence of Bad Pixels and the Efficacy of Two Mitigation Strategies", JWST-STScI-004324

Goudfrooij, P., et al. 2016, "NIRISS Operations Concepts: Target Acquisitions", JWST-STScI-004784

Holfeltz, S., Sivaramakrishnan, A., & Goudfrooij, P., 2015, "NIRISS Target Acquisition Centroid Simulations", JWST Technical Report JWST-STScI-003693

Holfeltz, S., Goudfrooij, P., & Sivaramakrishnan, A., 2015, "NIRISS Target Acquisition Centroid Simulations II: The Effects of Bad Pixels", JWST Technical Report JWST-STScI-003694

Perrin, M. D., Sivaramakrishnan, A., Lajoie, C.-P., Elliott, E., Pueyo, L., Ravindranath, S., & Albert, L., 2014, "Updated point-spead function simulations for JWST with WebbPSF", Proc. SPIE 9143

Sivaramakrishnan, A., & Artigau, É., 2014, "Aperture-Masking Interferometry with *Webb*'s NIRISS", STScI Newsletter, Vol. 31, Issue 01

Valenti, J., Regan, M., Balzano, V., & Koehler, R., 2013, "JWST Target Location Algorithm Description", JWST Technical Report JWST-STScI-001117